

# Journal of Biomedical Optics

BiomedicalOptics.SPIEDigitalLibrary.org

## **Selection of voxel size and photon number in voxel-based Monte Carlo method: criteria and applications**

Dong Li  
Bin Chen  
Wei Yu Ran  
Guo Xiang Wang  
Wen Juan Wu

# Selection of voxel size and photon number in voxel-based Monte Carlo method: criteria and applications

Dong Li,<sup>a</sup> Bin Chen,<sup>a,\*</sup> Wei Yu Ran,<sup>a</sup> Guo Xiang Wang,<sup>a,b</sup> and Wen Juan Wu<sup>a</sup>

<sup>a</sup>Xi'an Jiaotong University, State Key Laboratory of Multiphase Flow in Power Engineering, Xi'an 710049, China

<sup>b</sup>University of Akron, Department of Mechanical Engineering, Akron, Ohio 44325-3903, United States

**Abstract.** The voxel-based Monte Carlo method (VMC) is now a gold standard in the simulation of light propagation in turbid media. For complex tissue structures, however, the computational cost will be higher when small voxels are used to improve smoothness of tissue interface and a large number of photons are used to obtain accurate results. To reduce computational cost, criteria were proposed to determine the voxel size and photon number in 3-dimensional VMC simulations with acceptable accuracy and computation time. The selection of the voxel size can be expressed as a function of tissue geometry and optical properties. The photon number should be at least 5 times the total voxel number. These criteria are further applied in developing a photon ray splitting scheme of local grid refinement technique to reduce computational cost of a nonuniform tissue structure with significantly varying optical properties. In the proposed technique, a nonuniform refined grid system is used, where fine grids are used for the tissue with high absorption and complex geometry, and coarse grids are used for the other part. In this technique, the total photon number is selected based on the voxel size of the coarse grid. Furthermore, the photon-splitting scheme is developed to satisfy the statistical accuracy requirement for the dense grid area. Result shows that local grid refinement technique photon ray splitting scheme can accelerate the computation by 7.6 times (reduce time consumption from 17.5 to 2.3 h) in the simulation of laser light energy deposition in skin tissue that contains port wine stain lesions. © 2015 Society of Photo-Optical Instrumentation Engineers (SPIE) [DOI: [10.1117/1.JBO.20.9.095014](https://doi.org/10.1117/1.JBO.20.9.095014)]

Keywords: voxel-based Monte Carlo; grid size; photon number; local grid refinement; photon splitting.

Paper 150322RR received May 13, 2015; accepted for publication Aug. 31, 2015; published online Sep. 29, 2015.

## 1 Introduction

Adams and Wilson<sup>1</sup> were the first to adopt the Monte Carlo (MC) method in simulating photon transportation in biological materials with isotropic scattering of photons. Anisotropic scattering was later introduced into the MC for single-layered homogenous biological tissues by Prahl et al.<sup>2</sup> and Keijzer et al.<sup>3</sup> The MC modeling of light propagation in multilayered homogenous tissue (MCML) was developed by Wang et al.,<sup>4</sup> who incorporated light refraction and reflection on a planar interface between different layers into the simulation. MCML can also be used to deal with light propagation within a layered structure that contains simple geometric shapes, such as long cylinders, by using coordinate transformation,<sup>5</sup> geometrical analysis,<sup>6</sup> or delta-scattering technique.<sup>7</sup>

For complex structured tissue, the voxel-based Monte Carlo method (VMC) was proposed to deal with the light propagation in heterogeneous tissue.<sup>8–10</sup> In VMC, the actual nonhomogeneous tissue can be represented by a set of cubic material grid arrays (voxels). The light propagation within the tissue can be modeled as photons that continually interact with the boundary of the voxels. A good approximation of complex geometry can be provided, and the corresponding light propagation modeling is simple and flexible. Furthermore, this MC method can take structural information provided by magnetic resonance

imaging or x-ray computed tomography, which facilitates modeling light distribution in a real biological tissue.

However, avoiding artificial serrated polygonal boundary and significant errors in the simulation of light propagation in tissue with curved interface<sup>11</sup> is difficult for VMC. There are 2 main ways to solve this problem: increasing grid density or using tetrahedron mesh.<sup>10,12,13</sup> Regardless of the type of grid, an appropriate resolution of the grid system should be carefully chosen.<sup>14</sup> Low grid density may produce unacceptable error, whereas high grid density requires longer computation time and more computer memory. Therefore, optimizing the voxel size for VMC to satisfy the requirement of computational accuracy and efficiency is essential. An empirical guide on the voxel size selection can range from 10 to 20 microns in laser port wine stain (PWS) simulation. No theoretical criterion has ever been proposed to determine the minimum voxel size.

As a statistical method, the results of MC method are based on the average of multiple photons.<sup>8</sup> More photon numbers produce results that are more accurate. However, excessive photon numbers require tremendous computational time. Therefore, determining the minimum number of photons in actual MC simulation is important to achieve accurate results. However, the criterion for selecting the photon number in MC simulation is not available. The number of photons used in MC simulation is limited by either error estimation or computer capacity.

\*Address all correspondence to: Bin Chen, E-mail: [chenbin@mail.xjtu.edu.cn](mailto:chenbin@mail.xjtu.edu.cn)

To reduce computation time, certain improvements have been made to increase the efficiency of the MC method. Variance reduction technique<sup>15</sup> and parallel computations<sup>16</sup> were proposed to reduce the number of photons accurately. In variance reduction technique, a weight is assigned to each photon (or a photon package) upon entering the tissue. After energy absorption, the weight of the photon is reduced according to the probability of absorption rather than each photon undergoing termination after single absorption in the classic MC method. Patwardhan et al.<sup>17</sup> accelerated VMC by omitting the boundary calculations at every voxel interface. In their study, each photon step check for layer or object boundaries is conducted by comparing the refractive indexes of all the voxels within the photon path in each step size. Voxel crossing is calculated only if the refractive index changes along the photon path. Zolek et al.<sup>18</sup> found that the time-consuming computation in MC simulation is mainly associated with the calculation of the logarithmic and trigonometric functions, as well as the generation of pseudorandom numbers. In their study, the MC algorithm was optimized by approximating the logarithmic and trigonometric functions based on polynomial and rational functions. The approximated algorithm expedited the MC simulations by a factor of 4. Bhan and Spanier<sup>19</sup> replaced the exact probability model on which the conventional MC simulation is based by an approximate probability model. In this model, a large number of individual events are compressed into much fewer super-events; hence, simulations based on this approximation model are much faster. All these aforementioned improvements increased the computational efficiency of VMC. However, the computational burden is still large because of the unnecessarily dense grid and excessive photon number, which prevents further application of this method.

In this work, a criterion for the requirement on the minimum voxel size is established based on the energy absorption score principle and geometrical approximation of the curved structure. In addition, a second criterion for the minimum number of photons required by MC simulation is proposed by comparing the calculation result of light distribution within a homogenous medium in the MC method with that in a one-dimensional (1-D) analytical solution. A photon-splitting scheme with non-uniform grid is constructed based on the 2 criteria to increase the computational efficiency of VMC.

## 2 Criteria for the Determination of Voxel Size and Photon Number

In this section, the criteria for the maximum size of the control element (volume) and minimum photon number used in voxel-based MC simulation will be proposed. Although the problem is generally 3-dimensional (3-D), 1-dimensional (1-D) or 2-dimensional (2-D) cases are taken as examples because the light energy attenuation in skin tissue is mainly along the tissue depth, and the depth of the PWS lesion is much less than that of the surface area. The criteria will be validated by a 3-D VMC simulation of the light distribution during laser treatment of PWS.

To validate our code, we compared our result with other codes found in Ref. 20 in terms of diffuse reflectance/transmittance. We compared the results of MC simulation of diffuse reflectance Rd and transmittance Td for a scattering slab illuminated by normally incident collimated light with the results tabulated by van de Hulst,<sup>21</sup> the results of adding-doubling method obtained by Prahil,<sup>22</sup> the results of MCML developed by Wang et al.,<sup>4</sup> and the results of O<sup>3</sup>MC developed by Doronin and

Meglinski.<sup>20</sup> The following parameters of slab have been used in the simulation: scattering coefficient  $\mu_s = 9 \text{ mm}^{-1}$ , absorption coefficient  $\mu_a = 1 \text{ mm}^{-1}$ , anisotropic factor  $g = 0.75$ , refraction coefficient  $n = 1$ , and slab thickness  $d = 0.2 \text{ mm}$ . All the comparison results are listed in Table 1, which proved that our code is reliable.

### 2.1 Criterion for Voxel Size Selection

#### 2.1.1 Criterion based on geometrical approximation

In the VMC method, the curved interfaces are approximated by the boundary of the voxel. As shown in Fig. 1, the cross-section of a cylindrical blood vessel (vessel diameter  $d = 120 \mu\text{m}$ ) is approximated by regular voxels (red blocks in Fig. 1). If the voxel size is large,  $d/6$  for example [Fig. 1(a)], then the approximate interface significantly deviates from the curve, which results in a deviation of the vessel area in the discretized domain. Consequently, a large error exists when the photons refract or reflect on the vessel wall. As the voxel size is reduced to  $d/12$  [Fig. 1(b)] and  $d/24$  [Fig. 1(c)], the serrated polygonal boundary is smoothed, and the cross-section area approaches the real vessel.

For consistency, a dimensionless parameter is defined as  $\lambda = d^*/\Delta w^*$ , where  $d^* = d \cdot \mu_t$  is the dimensionless length and  $\Delta w^* = \Delta w \mu_t$  is the dimensionless voxel width. For a circular blood vessel cross-section, the ratio of the voxel-generated blood vessel area (red part in Fig. 1) to the real blood vessel area (area within dashed black lines in Fig. 1) is then related to  $\lambda$  as indicated in Fig. 2. As can be seen, the area ratio quickly approaches 1 with increasing  $\lambda$ . If  $\lambda$  is  $>10$ , then the area ratio changes very little ( $<3\%$ ), and the relationship is true for all 3 vessel diameters (60, 120, and  $180 \mu\text{m}$ ). Therefore,  $\lambda = 10$  can be used as a criterion from the geometrical point of view by which the dimensionless voxel width is given.

$$\Delta w^* = 0.1d^*. \quad (1)$$

This criterion applies beyond the circular interface. For the irregular curved interface, the dimensionless diameter  $d^*$  in Eq. (1) can be determined as  $d^* = 2\mu_t/K_{\max}$ , where  $K_{\max}$  is the maximum curvature of the curved interface.

#### 2.1.2 Criterion based on geometrical approximation

A laser beam that propagates through a homogeneous medium with uniform absorption and scattering properties, as shown in

**Table 1** Comparison of the diffuse reflectance Rd and transmittance Td given by van de Hulst,<sup>21</sup> the adding-doubling method by Prahil,<sup>22</sup> the MCML developed by Wang et al.,<sup>4</sup> the O<sup>3</sup>MC developed by Doronin and Meglinski,<sup>20</sup> and the proposed voxel-based Monte Carlo method.

Reference	Rd	Error	Td	Error
21	0.09739	—	0.66096	—
4	0.09734	0.00035	0.66096	0.0002
22	0.09711	0.00033	0.66159	0.00049
20	0.09741	0.00027	0.66096	0.00017
Proposed	0.09735	0.00034	0.66096	0.00018

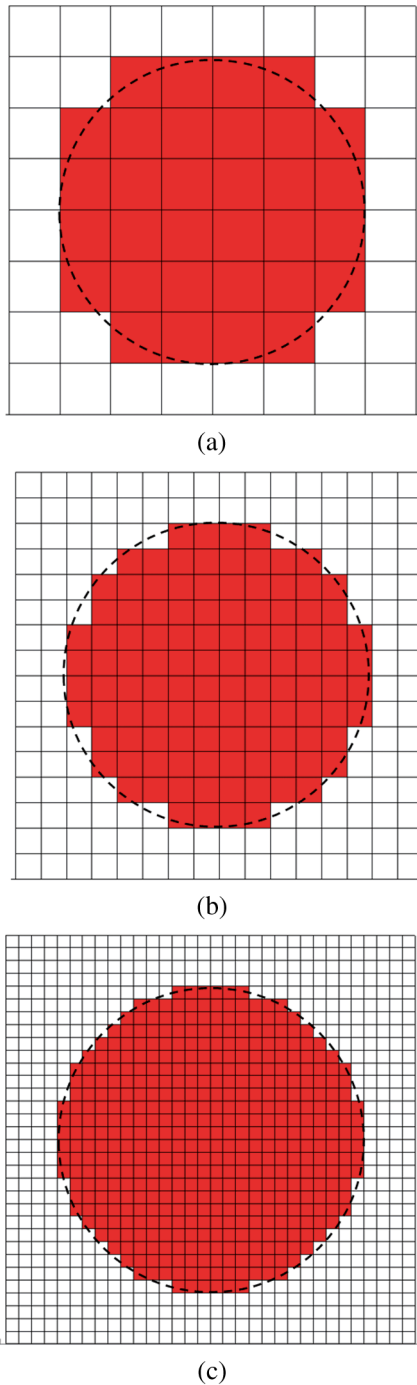


**Fig. 1** Representation of blood vessel cross-section with a diameter of  $120\ \mu\text{m}$  by voxels when the voxel size is (a)  $d/6$ , (b)  $d/12$ , and (c)  $d/24$ .

Fig. 3, is considered. For the light with fluence of  $F_0$  at the incident point  $o$ , the analytical solution of light fluence  $F(w)$  at the depth of  $w$  within the medium can be assumed to be attenuated in the skin tissue as the consecutive black solid line in Fig. 3 and presented according to the Beer-Lambert law as follows:

$$F(w) = F_0 \cdot \exp(-\mu_t w), \quad (2)$$

where  $\mu_t$  is the attenuation coefficient of the medium. In a high absorbing medium,  $\mu_t = \mu_a$  (e.g., blood). In a high scattering

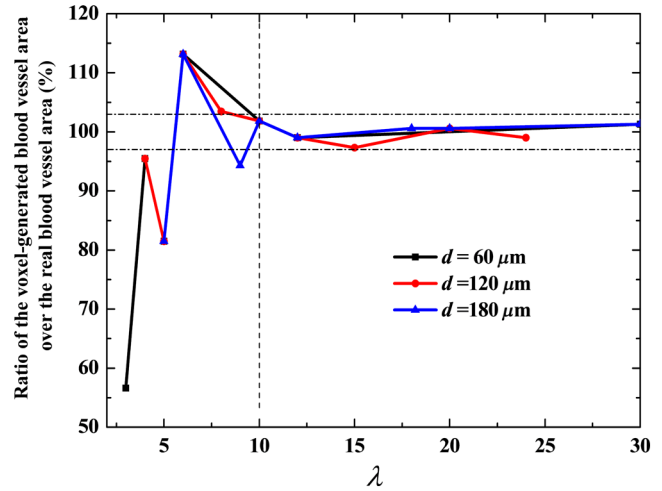


**Fig. 2** Relationship between  $\lambda$  and the ratio of the generated blood vessel area to the real blood vessel area.

medium defined by the diffusion theory,  $\mu_t = \{3\mu_a \times [\mu_a + (1-g)\mu_s]\}^{1/2}$  (like the situation in epidermis and dermis).  $\mu_a$ ,  $\mu_s$ , and  $g$  are the absorption coefficient, scattering coefficient, and anisotropic factor, respectively.<sup>4</sup>

To calculate light attenuation with the MC method, a grid system has to be constructed to score the energy deposition in each grid cell (voxel) discretely. In this case, the medium can be discretized into cells of width  $\Delta w$  (assuming a uniform grid). The coordinates at the grid interface  $ws_i$  ( $i = 1$  to  $k$ ,  $k$  is the node index of the last element) and the cell center  $w_i$  ( $i = 1$  to  $k$ ) can then be easily determined by

$$\Delta w = ws_{i+1} - ws_i = w_{i+1} - w_i. \quad (3)$$

During the calculation, the photon weight absorbed within the cell (control volume) would be stored in each cell. After sufficient photon traveling, the calculated light fluence would be presented discretely as an array  $\bar{F}(w_i)$  (zigzag red line shown in Fig. 3).  $\bar{F}(w_i)$  can be calculated based on the energy (area under both lines) conservation with analytical solution over the domain of each cell  $i$ .

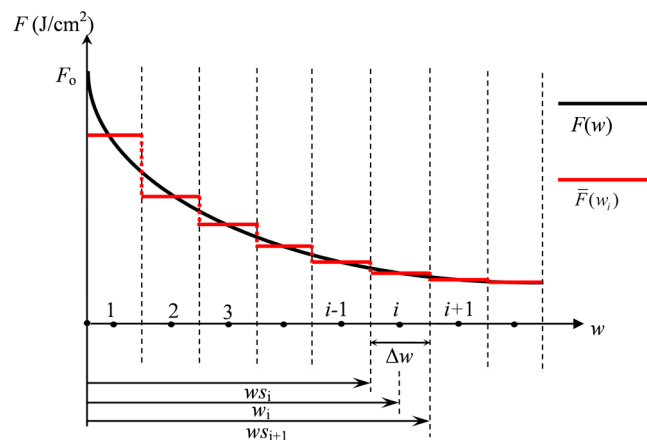


**Fig. 3** Schematic of light attenuation and grid separation in homogeneous medium.

$$\bar{F}(w_i)\Delta w = \int_{w_i-\Delta w/2}^{w_i+\Delta w/2} F(w)dw. \quad (4)$$

Integrating Eq. (2) into Eq. (4), we obtain

$$\begin{aligned} \bar{F}(w_i) &= \frac{F_o \times \int_{w_i-\Delta w/2}^{w_i+\Delta w/2} \exp(-\mu_t w)dw}{\Delta w} \\ &= \frac{F_o \times \exp(-\mu_t w_i)[\exp(\mu_t \Delta w/2) - \exp(-\mu_t \Delta w/2)]}{\Delta w \cdot \mu_t}. \end{aligned} \quad (5)$$

However, if the light attenuation is large within the grid domain, then the scored light fluence may deviate from the analytical solution, particularly at the cell interface, although the energy conservation in each grid domain can be achieved. For example, the light attenuation is obvious in the first cell (Fig. 3). As a result, the scored light fluence in the first cell  $\bar{F}(w_1)$  is much lower than the analytical solution  $F(w)$  at the first cell interface  $ws_1$ , as shown in Fig. 3. To diminish such difference and increase the accuracy and sensitivity of the MC result, the grid cell width should ensure that the scored light fluence  $\bar{F}(w_i)$  in the  $i$ 'th cell is not significantly lower than the analytical solution of light fluence at the cell interface  $ws_{i-1}F(ws_{i-1})$ . An approximation factor  $\delta$  ( $0 < \delta < 1$ ) is then introduced and defined as

$$\begin{aligned} \delta &= \frac{\bar{F}(w_i)}{F(ws_i)} \\ &= \frac{F \times \exp(-\mu_t w_i)[\exp(\mu_t \Delta w/2) - \exp(-\mu_t \Delta w/2)]}{\Delta w \cdot \mu_t} / \\ &\quad \times \left\{ F \cdot \exp\left[-\mu_t \left(w_i - \frac{w}{2}\right)\right] \right\} = \frac{1 - \exp(-\Delta w \mu_t)}{\Delta w \mu_t}. \end{aligned} \quad (6)$$

A dimensionless cell width is defined,  $\Delta w^* = \Delta w \mu_t$ , which is the ratio of the cell width  $\Delta w$  to the light penetration depth  $1/\mu_t$  in the medium. Equation (6) then becomes

$$\delta = \frac{1 - \exp(-\Delta w^*)}{\Delta w^*}. \quad (7)$$

$\delta$  implies the approximation of the simulated result by the MC method to the analytical solution. A high value of  $\delta$  must be achieved to ensure the computational accuracy of MC. For instance,  $\delta \geq 0.9$  means that the computational error by MC simulation compared with that of the analytical solution is  $<10\%$ . As can be seen in Eq. (6), as the criterion, the corresponding  $\Delta w^*$  approaches 0.2, as

$$\Delta w^* = 0.2. \quad (8)$$

This criterion is introduced based on the light energy scoring independent of the photon movement. Therefore, this criterion is applicable to any MC method.

In summary, 2 factors affect the selection of voxel size in the VMC method: the discretization of irregular geometry [Eq. (1)] and the discretization of light propagation [Eq. (8)]. These 2 equations are plotted in Fig. 4. As can be seen, if the dimensionless diameter  $d^*$  is  $<2$ , then the voxel size is dominated by the geometric approximation of the curved interface [Eq. (1)]. Otherwise, the voxel size is dominated by the optical property

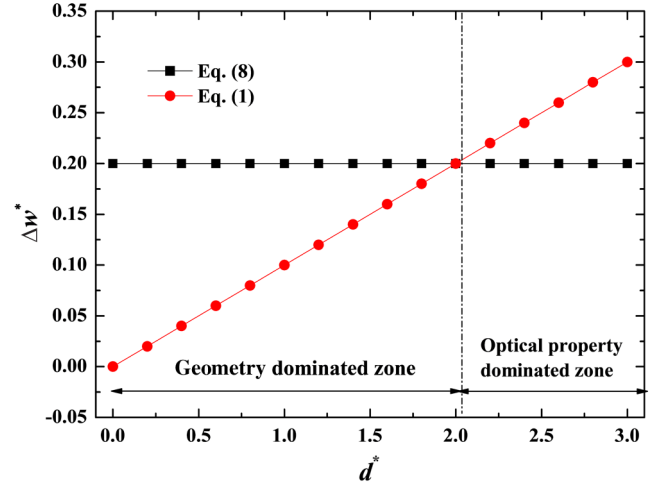


Fig. 4 Relationship of  $\Delta w^*$  and  $d^*$ .

of the medium [Eq. (8)]. Finally, these 2 factors can be considered in the following unified expression:

$$\begin{cases} \Delta w^* = 0.1d^* & d^* \leq 2 \\ \Delta w^* = 0.2 & d^* \geq 2 \end{cases}. \quad (9)$$

Notably, the attenuation coefficient of the medium is incorporated into the nondimensional voxel width,  $\Delta w^* = \Delta w/(1/\mu_t)$ . The attenuation coefficient significantly affects the real size of the voxel. In a high absorbing medium,  $\mu_t = \mu_a$  (e.g., blood). As a result, the voxel size is independent with scattering properties. On the other hand, in a high scattering medium,  $\mu_t = \{3\mu_a \times [\mu_a + (1-g)\mu_s]\}^{1/2}$  (like the situation in epidermis and dermis). The voxel size is highly related to scattering properties. The local voxel size should be small with high scattering coefficient and large with low scattering coefficient. As for the medium with nonuniform scattering properties, the nonuniform grid should be used.

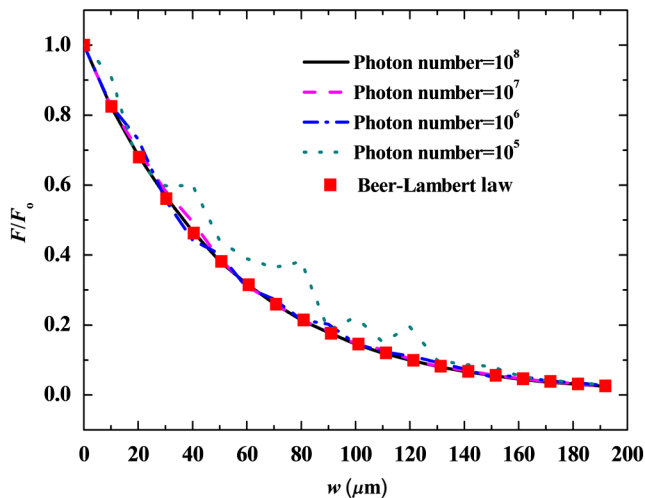
## 2.2 Criterion for the Determination of Photon Number

In MC simulation, the number of photons should be sufficiently large to satisfy the statistical requirement at the given voxel.<sup>8</sup> The number of photons that arrived at each voxel depends on the total photon number in the simulation and the voxel size. For a coarse grid with a large cell size, a small number of photons may produce sufficient photons for each voxel. However, a small voxel should be used for a medium with large attenuation coefficients (either absorption or scattering), as shown in Eq. (9). The number of photons that arrive at each voxel will then become smaller if the same number of total photons is used, which may not meet the basic requirement of statistics and will lead to large simulation errors.

To demonstrate the effect of the photon number on the simulation result, a comparison of the light fluence distribution by the MC method with that by the analytical solution (Beer-Lambert law) was performed for a 1-D photon propagation problem within a homogeneous medium (blood) with uniform optical properties. The wavelength of the laser is 585 nm. The optical properties of the blood are listed in Table 2.<sup>8</sup> As illustrated in Fig. 5, the MC method agrees well with the analytical solution when the total photon number is  $>10^7$ . A large error

**Table 2** Optical properties of skin components.<sup>8</sup>

Properties	Epidermis	Dermis	Blood
Thermal conductivity $\lambda$ (kW/m · K)	0.34	0.41	0.55
Specific heat $c$ (J/kg · K)	3200	3500	3600
Absorption coefficient $\mu_a$ (cm <sup>-1</sup> )	20	2.4	191
Scattering coefficient $\mu_s$ (cm <sup>-1</sup> )	470	129	467
Anisotropy index $g$	0.79	0.79	0.99
Refractive index $n$	1.37	1.37	1.33


**Fig. 5** Comparison of analytical solution and Monte Carlo (MC) simulation result with various photon numbers.

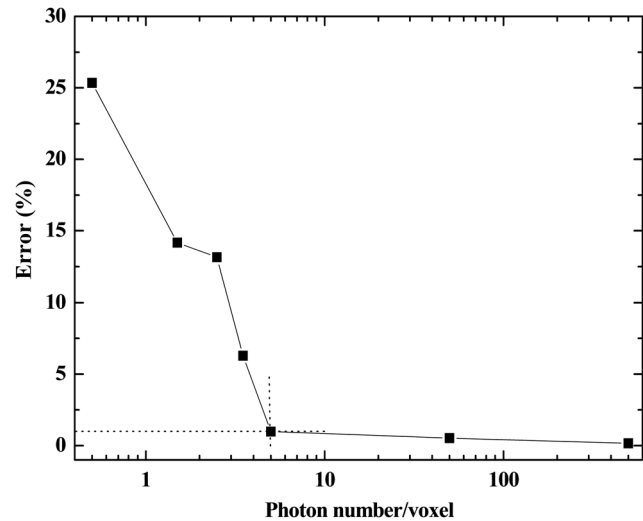
can be observed for the case with a photon number of  $10^5$ . The relative error of the MC method from the analytical solution can be plotted as a function of the photon number per voxel in Fig. 6. Interestingly, the error has a close relationship with the number of photon per voxel. Two regions show different dependences between the 2 variables. When the number of photons per voxel is  $<5$ , the MC method produces greater error. However, when the number is  $>5$ , the error produced by the MC method decreases. Further increasing the photon number per voxel will not significantly improve the accuracy of the MC method.

Apparently, 5 photons per voxel can control the selection of the total photons in the MC simulation. The 5 photons per voxel can be used as the basic requirement for the minimum photons required by the MC simulation, that is, the total photons required by the MC simulation will be 5 times that of the voxels in the simulation.

### 2.3 Criterion Validation

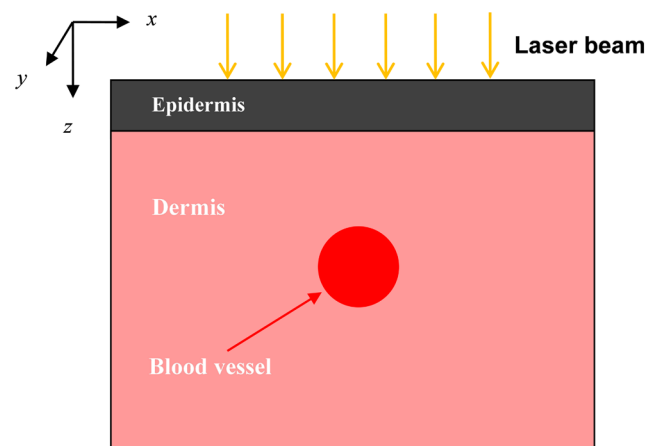
The in-house VMC code is written by using MATLAB®, and the validation of the code can be seen in a previous study.<sup>13</sup> The light propagation during laser treatment of PWS is taken as an example to validate the above criteria of voxel size and photon number.

PWS birthmarks are congenital vascular malformations that occur in  $\sim 0.3\%$  of newborns. PWS is composed of ectatic


**Fig. 6** Relation of computation error by MC with photon number per voxel.

venular capillary blood vessels, with diameters that range from 10 to 300  $\mu\text{m}$ , buried within healthy dermal tissue. PWS can be treated by pulsed dye laser with wavelength in the visible band (e.g., 585 nm) based on the theory of selective photothermolysis, with hemoglobin serving as the target chromophore.<sup>23</sup> According to the theory, the PWS blood vessels can be thermally damaged selectively because of their preferential absorption of laser energy compared with normal skin tissues, which are minimally affected.

The skin that contains PWS can be assumed as a 2-layer geometry composed of epidermis and dermis layers, as shown in Fig. 7. A single PWS blood vessel that comprises highly absorbing blood is considered, buried in the center of the dermis and parallel to the skin surface. The dimensions of the computational skin model are  $x_k \times y_k \times z_k = 1440 \mu\text{m} \times 1440 \mu\text{m} \times 1020 \mu\text{m}$ . The thicknesses of the epidermis and dermis are 60 and 960  $\mu\text{m}$ , respectively. The diameter of the blood vessel is 120  $\mu\text{m}$ , and the depth of the vessel center to the skin surface is 250  $\mu\text{m}$ . A typical PWS treatment wavelength of 585 nm is used, as shown in Table 2.<sup>8</sup> The circular laser beam is fired in the center of the skin surface, with a diameter of 1000  $\mu\text{m}$ .


**Fig. 7** Schematic of the 2-layer skin model containing port wine stain.

For such skin tissue with PWS, the attention should be on the blood vessel. Based on the criterion, for the blood vessel with a diameter of  $120\ \mu\text{m}$ ,  $d^* = 120\ \mu\text{m} \times 191 / (10^4\ \mu\text{m}) = 2.292$ . As a result, the voxel size for the blood vessel  $\Delta w = 0.2 / (191 \times 10^{-4}) = 10.47\ \mu\text{m}$ . To test for reasonability, the effect of the voxel size on the light attenuation within a blood vessel along the centerline of the laser spot is examined. The voxel size is selected as 5, 10, and  $20\ \mu\text{m}$ , the cell numbers are  $288 \times 288 \times 204$ ,  $144 \times 144 \times 102$ , and  $72 \times 72 \times 51$ , respectively, and the corresponding photon numbers are  $5 \times 10^6$ ,  $4 \times 10^7$ , and  $6.25 \times 10^5$ , all of which meet the requirement for the total number of photons. As can be seen from Fig. 8, the highest energy density predicted with the voxel size of  $20\ \mu\text{m}$  ( $136\ \text{J}/\text{cm}^3$ ) is significantly lower than those with the voxel size of either  $10\ \mu\text{m}$  ( $167\ \text{J}/\text{cm}^3$ ) or  $5\ \mu\text{m}$  ( $173\ \text{J}/\text{cm}^3$ ). At the same time, the calculation result with a cell size of  $10\ \mu\text{m}$  is  $167\ \text{J}/\text{cm}^3$ , which is close to the result with a cell size of  $5\ \mu\text{m}$  ( $173\ \text{J}/\text{cm}^3$ ).

The energy deposition with cell size of  $1\ \mu\text{m}$  is the basic solution, and the simulated result is compared with that of a larger cell size from 2 to  $80\ \mu\text{m}$ . The computation error of the maximum energy deposition within the blood vessel is illustrated in Fig. 9 as a function of the cell size. The computation error becomes smaller as the cell size decreases. The computation error is  $>10\%$  when the voxel size is  $>10\ \mu\text{m}$ . Therefore, the largest cell size for the  $120\text{-}\mu\text{m}$  blood vessel with a wavelength of  $585\ \text{nm}$  is  $10\ \mu\text{m}$ , which is consistent with the above criterion.

The effect of the total photon number on the light density distribution in the blood vessel is shown in Fig. 10, with the voxel size of  $20\ \mu\text{m}$  [Fig. 10(a)] and  $5\ \mu\text{m}$  [Fig. 10(b)]. The minimum number of photons based on the requirement of 5 per voxel is  $6.25 \times 10^5$  and  $4 \times 10^7$  for 20 and  $5\ \mu\text{m}$ , respectively. The results from different photon numbers ( $10^5$  to  $10^7$  for  $20\ \mu\text{m}$  voxels and  $10^6$  to  $10^8$  for  $5\ \mu\text{m}$  voxels) are also plotted in the same figures. By comparison, if the total number of photons is less than the corresponding minimum number, then the calculated results show significant deviation from those results with more photons. For example, in the case of  $20\ \mu\text{m}$  voxels [Fig. 10(a)], 2 results with a photon number larger than the minimum number ( $6.25 \times 10^5$ ) agree fairly well with that which uses the minimum photon number ( $6.25 \times 10^5$ ), whereas the result

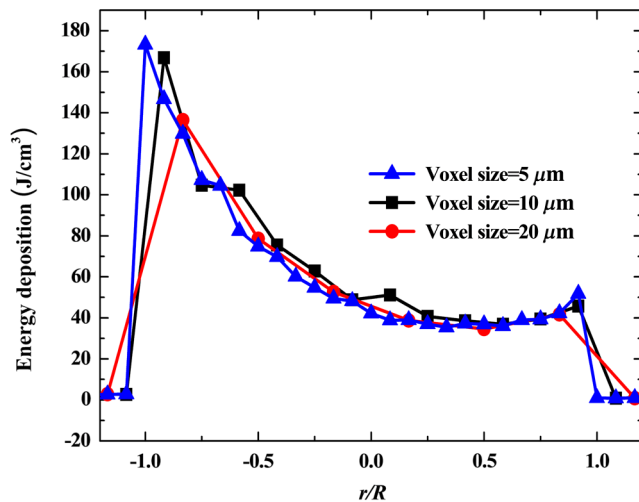


**Fig. 8** Light attenuation within a blood vessel along the centerline of the laser spot with voxel size of 5, 10, and  $20\ \mu\text{m}$ .

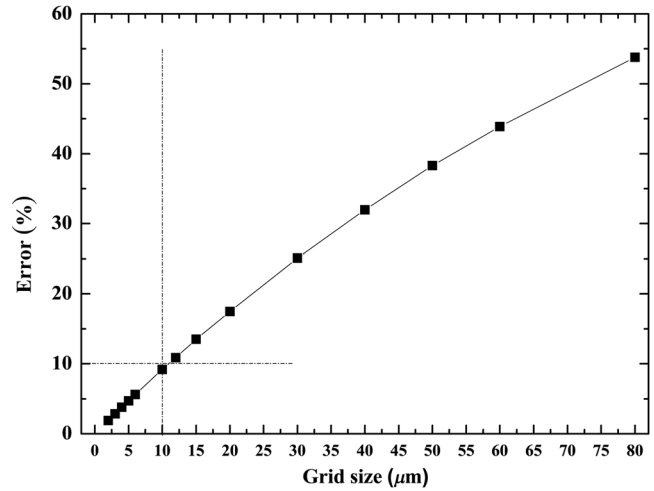
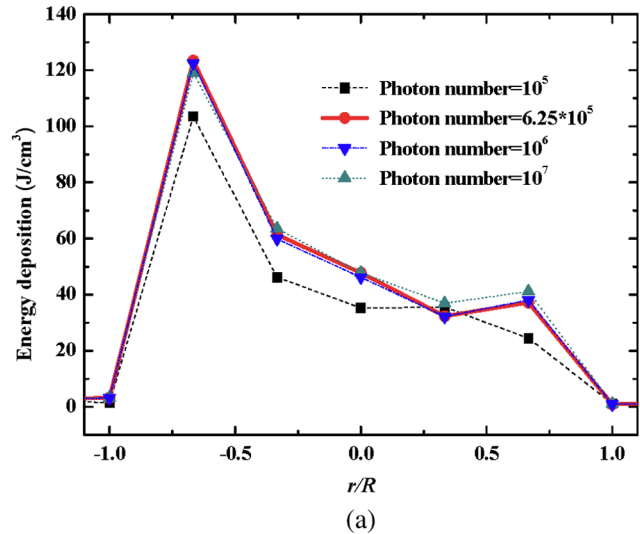
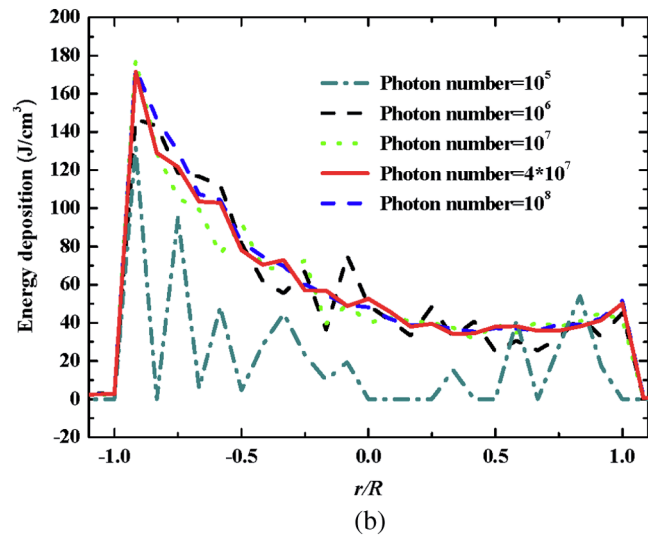


**Fig. 9** Computation error of the maximum light energy deposition within blood vessel as a function of grid size from 2 to  $80\ \mu\text{m}$ .



(a)



(b)

**Fig. 10** Energy deposition within blood vessel along tissue depth at the laser spot center with voxel size of (a)  $20\ \mu\text{m}$  and (b)  $5\ \mu\text{m}$  with various photon numbers.

for photon number of  $10^5$  significantly deviates from the other results. Similar results can be observed in the case of  $5 \mu\text{m}$  voxels [Fig. 10(b)]. All the results with photons less than the minimum required number ( $4 \times 10^7$ ) show large fluctuations and significantly deviate from the results with large photons. A further increase in the photons beyond the minimum requirement makes no significant improvement. This comparison confirms the conclusion from the 1-D analysis, and the requirement for the number of photons for MC simulation, which is 5 photons per voxel, seems reasonable.

### 3 Nonuniform Grid System and a Photon Splitting Scheme

#### 3.1 Local Grid Refinement and Photon Splitting Technique

Based on the criterion in Eq. (9), the voxel size used in a 3-D VMC is greatly affected by the optical properties of the medium. For a system that consists of various tissue components with vastly different optical properties, the voxel size should be determined by the tissue component with the largest attenuation coefficient (such as blood vessel in PWS) if a uniform grid is used. For such a fine grid, a significant number of photons should also be used to satisfy the criteria for photon selection (5 times the number of voxels in the simulation) to guarantee computational accuracy. However, a coarse grid and fewer photons can be used for tissue components with less absorption, such as dermis.

Although the nonuniform grid is widely used in numerical simulations,<sup>24,25</sup> the uniform grid is usually used in MC simulation, at least for the simulation of laser-tissue interactions.<sup>8,26–28</sup> In this section, a nonuniform grid system is proposed to save computational cost. Aside from this nonuniform grid system, the photon splitting scheme is also developed to increase the photon number needed to satisfy the statistical accuracy requirement of 5 photons per voxel in the dense grid area. A 2-layer skin model that contains a single PWS blood vessel (Fig. 7) is taken as an example to illustrate the nonuniform grid system and photon splitting scheme.

First, the tissue interfaces should be defined to distinguish different grid densities. Two interfaces are in the 3 tissue components, that is, the epidermis-dermis interface and dermis-blood vessel interface. For simplicity, a rectangular cylinder is constructed to enclose the blood vessel as the dermis-blood vessel interface is curved. In the rectangular cylinder region that contains the blood vessel, a dense grid is determined based on the blood optical property by using the criterion in Eq. (9). The other domain of dermis can then be discretized by the coarse grid with a large voxel, with the width determined based on the dermis optical property. By contrast, the epidermis can have its own voxel size through the criterion. The schematic of the 2-D final grid for entire computational domain is shown in Fig. 11(a). The area within the dashed region is the blood vessel, which is represented by the discrete square voxels. For simplicity, the voxel size of the epidermis and dermis is the same.

Aside from the nonuniform grid system, a photon splitting scheme is suggested. For the nonuniform grid system shown in Fig. 11(a), the total number of photons used in the MC simulation can be determined based on the large voxels in the dermis, that is, 5 times the total number of large voxels. When a photon travels from the coarse grid into the fine one, the photon will be split into  $n$  subphotons (either inside or outside the dense grid). As shown in Fig. 11(b),  $n$  is determined based on the

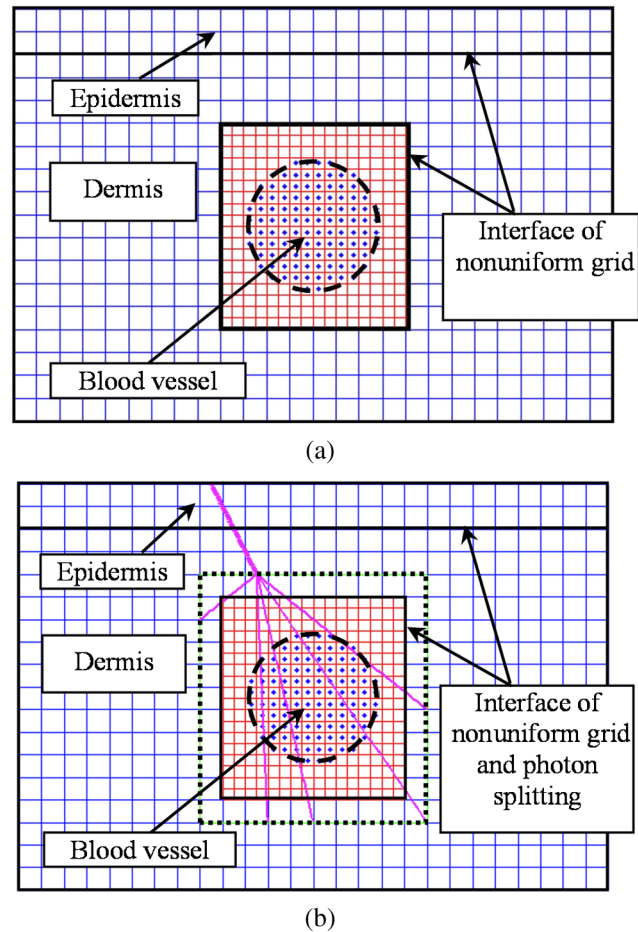


**Fig. 11** Schematic of (a) nonuniform grid system and (b) photon splitting.

requirement of the photon numbers for statistical accuracy of the fine grid, that is, at least 5 photons per voxel. Then, all  $n$  subphotons will be examined before a new photon is projected on the surface again.

#### 3.2 Effect of Local Grid Refinement and Photon Splitting Technique

The main objective of the nonuniform grid system and the photon splitting scheme is to reduce computational cost while maintaining accuracy. The single blood vessel skin model (Fig. 7) will be used to demonstrate the improvement of computation efficiency by the nonuniform grid system and the photon splitting scheme.

Based on Eq. (9), the maximum voxel size can be determined for each skin component. For the blood vessel with a diameter of  $120 \mu\text{m}$ ,  $d^* = d\mu_t = 120 \mu\text{m} \times 191 / (10^4 \mu\text{m}) = 2.23$ ; then the maximum voxel size should be  $\Delta w = 0.2 / \mu_t = 10.47 \mu\text{m}$ . For the epidermis with planar interface, the maximum voxel size  $\Delta w = 0.2 / \mu_t = 0.2 / 79.38 = 25.19 \mu\text{m}$ . For the dermis, similar to the epidermis, the maximum voxel size  $\Delta w = 0.2 / \mu_t = 0.2 / 13.9 = 143.9 \mu\text{m}$ .

The light transportation in skin tissue and blood vessel was calculated with a uniform grid throughout the entire computational domain, with the voxel size determined by the requirement for the blood vessel because the finest voxels are needed in the blood vessel. The voxel size and the photon

number are  $10\ \mu\text{m}$  and  $10^7$ , which has been used in the Ref. 8. The computation was completed in 17.5 h (CPU time) by HP xw6600 Workstation. The average energy density of the entire blood vessel area is  $77.31\ \text{J}/\text{cm}^3$ .

The result of the nonuniform grid was then checked. Voxel size is fixed for the epidermis ( $20\ \mu\text{m}$ ) and the rectangular dense grid area that contains the blood vessel ( $10\ \mu\text{m}$ ), but the dermis has different voxel sizes from  $10$  to  $80\ \mu\text{m}$  where the absorption is small and a large voxel size can be used, and the total number of photons is maintained at  $10^7$ . The computational time is reduced from 17.5 to 5.5 h when the voxel size in dermis was increased from  $10$  to  $80\ \mu\text{m}$  by the same workstation, as shown in Fig. 12. The figure also indicated that a further increase in voxel size in dermis would not further reduce the computational time. By contrast, increasing the voxel size in dermis also increases the computational error of the total energy density in the blood vessel, as shown in Fig. 13, although the overall error is within 3%. A coarse grid in the dermis shows no effect on the energy density distribution in the blood vessel, as shown in Fig. 14, which provides the light distributions within the blood vessel for 2 cases with dermis voxel sizes of  $20\ \mu\text{m}$  [Fig. 14(a)] and  $80\ \mu\text{m}$  [Fig. 14(b)], respectively.

For the fixed voxel size of  $20\ \mu\text{m}$  in the epidermis,  $80\ \mu\text{m}$  voxel in the dermis, and  $10\ \mu\text{m}$  voxel for the rectangular dense grid area that contains the blood vessel, the computational time can be further reduced from 5.5 hours to 3.5 and 2.3 h by reducing the total photon number from  $10^7$  to  $10^6$  and  $10^5$ , which correspond to the splitting number  $n$  from 1 to 10 and 100, as shown in Fig. 15. Both photon numbers satisfy the photon requirement for fine grid (blood vessel area).

Figure 16 shows the effect of the splitting number  $n$  on the accuracy of the simulation results, which is represented by the percentage of the difference from the average energy density calculated by using the finest uniform grid (voxel size of  $10\ \mu\text{m}$ ) for the entire computation domain and the total photon number  $10^7$ . The error introduced by photon splitting is relatively small ( $<5\%$ ), which demonstrates that the present photon splitting technique is valid and maintains energy conservation. The light deposition within the grid refinement area with  $n = 10$  and  $n = 100$  are plotted in Figs. 17(a) and 17(b). Photon splitting in the fine grid area shows no effect on the energy density distribution in the blood vessel, as shown in Fig. 17.

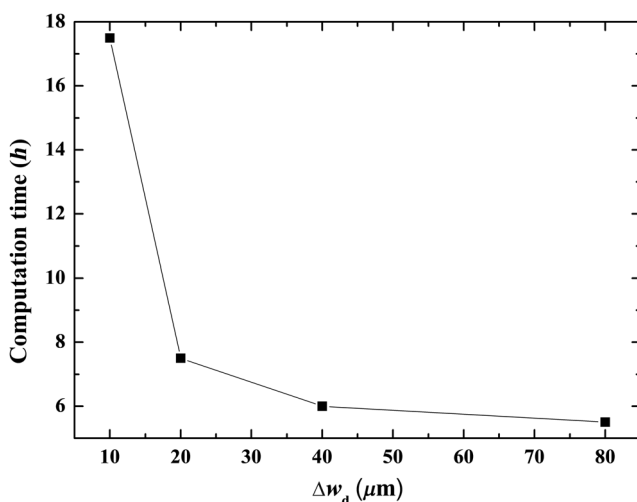


Fig. 12 Relation between computation time and voxel size in dermis.

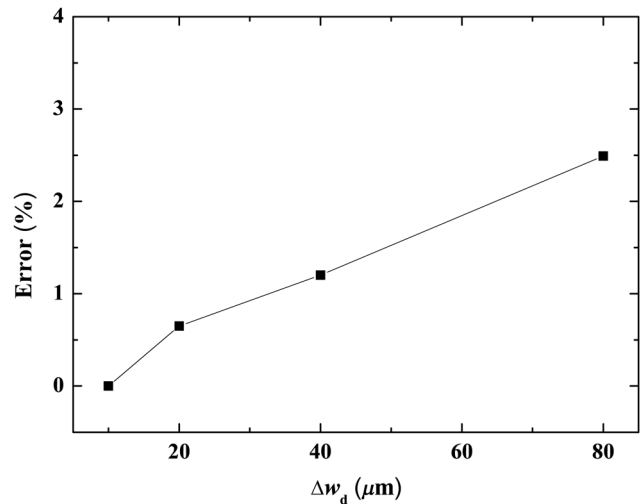


Fig. 13 Error of total energy density in the blood vessel as a function of voxel size in dermis.

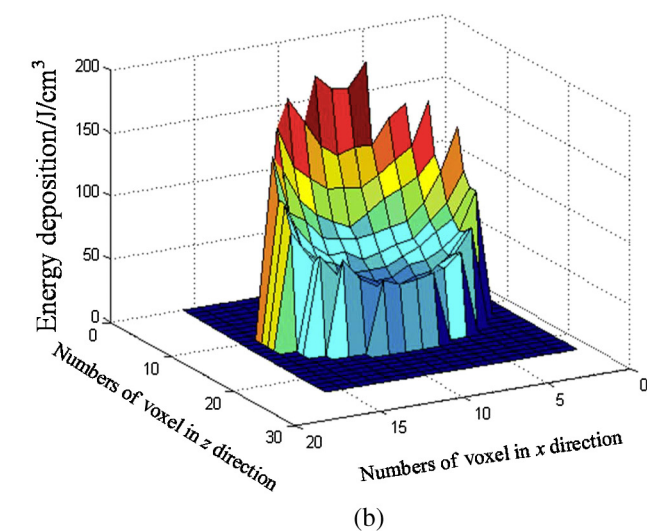
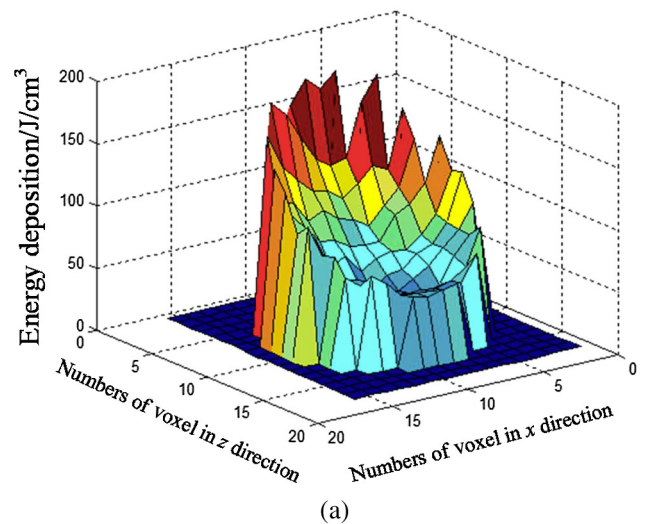


Fig. 14 Energy density in refined area with dermis grid size of (a)  $20\ \mu\text{m}$  and (b)  $80\ \mu\text{m}$ .

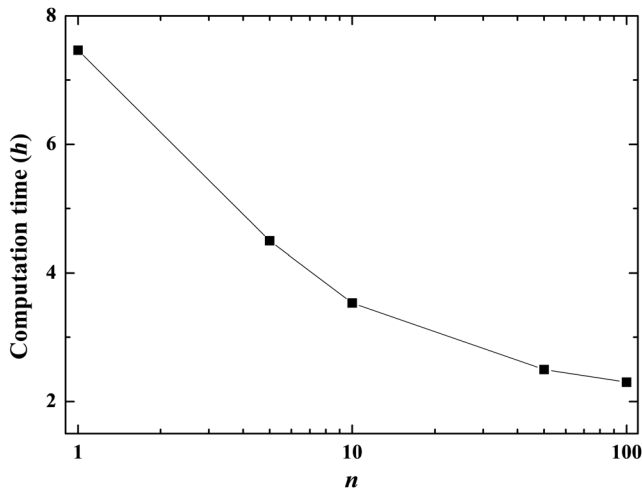


Fig. 15 Relation between splitting number  $n$  and computation time.

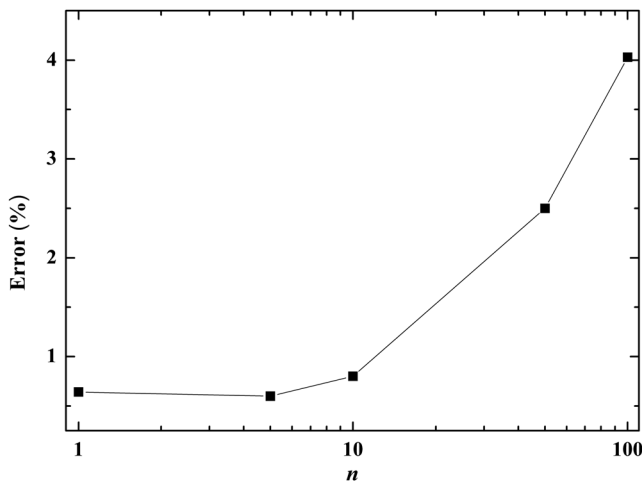


Fig. 16 Error in the energy density in the blood vessel as a function of splitting number.

#### 4 Conclusion

VMC has been proven effective in simulating light propagation and energy deposition in heterogeneous biological tissue with complex geometry. However, the criteria for selection of cell size and photon number had not been discussed yet. On one hand, if the cell size is too small, more photons are needed for simulation and the computation would be expensive. On the other hand, the accuracy of the simulation result cannot be guaranteed if the cell size is too large or if the photon number is not sufficiently large.

In this paper, criteria are proposed for the selection of the voxel size and the photon number in VMC simulation. Selection of the voxel size can be expressed as follows:

$$\begin{cases} \Delta w\mu_t = 0.1d\mu_t & d\mu_t \leq 2 \\ \Delta w\mu_t = 0.2 & d\mu_t \geq 2 \end{cases} \quad (10)$$

Selection of the photon number is highly related to the number of voxels. The photon number should be at least 5 times the total voxel number.

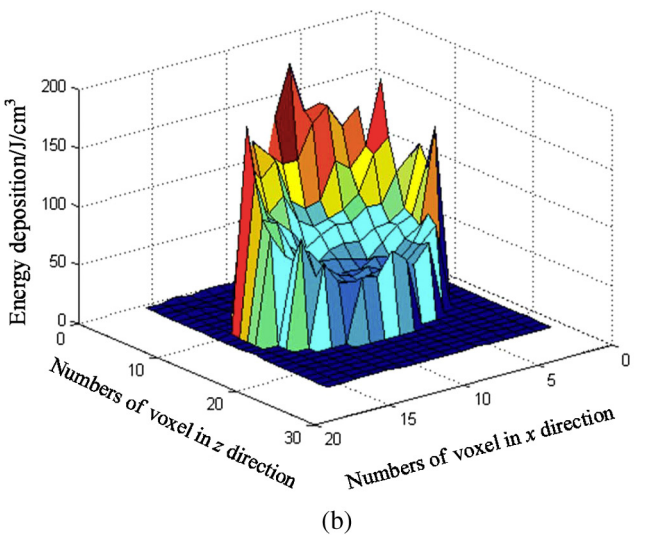
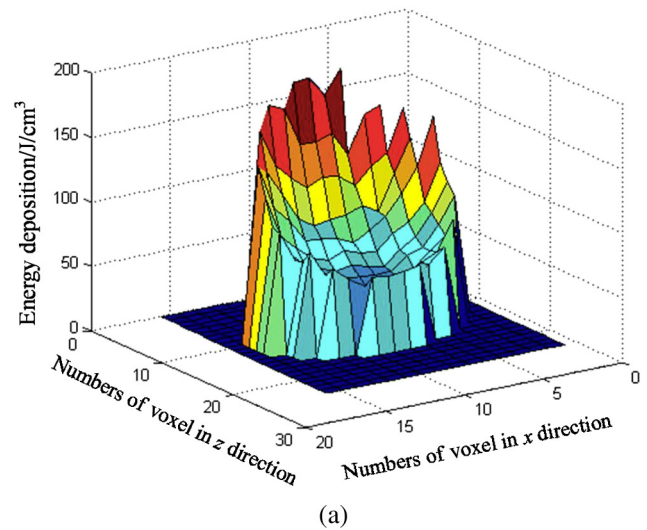


Fig. 17 Energy distribution within refined area with splitting number of (a) 10 and (b) 100 (voxel size: epidermis  $20 \mu\text{m}$ , unrefined dermis  $80 \mu\text{m}$ , and refined area  $10 \mu\text{m}$ ).

Based on the criterion, a photon ray splitting scheme of local grid refinement technique to expedite the VMC method was developed for the case of a nonuniform tissue structure with significantly varying optical properties. In the proposed technique, a local refined grid system is used in the nonuniform tissue structure, where fine grids are used for the tissue with high absorption and complex geometry and coarse grids for the other part. The total photon number is selected based on the coarse grid size, and the photon splitting scheme is developed to satisfy the statistical accuracy requirement for the dense grid area when the photons enter the fine grid from the coarse grid.

According to our study, the time consumption of the VMC in a 2-layer skin model that contains a single blood vessel can be greatly reduced from 17.5 to 2.3 h (accelerated by 7.6 times) in the simulation of the laser light energy deposition in skin tissue that contains PWS lesions based on this local refinement technique photon ray splitting scheme.

#### Acknowledgments

This work is supported by the National Natural Science Foundation of China (51336006), the International Science &

Technology Cooperation Plan of Shaanxi Province (2013KW30-05), and Fundamental Research Funds for the Central Universities.

## References

1. B. C. Wilson and G. Adam, "A MC model for the absorption and flux distributions of light in tissue," *Med. Phys.* **10**, 824–830 (1983).
2. S. A. Prahl et al., "A Monte Carlo model of light propagation in tissue," SPIE Institute Series IS 5, 102–111 (1989).
3. M. Keijzer et al., "Light distributions in artery tissue: MC simulations for finite-diameter laser beams," *Lasers Surg. Med.* **9**, 148–154 (1989).
4. L. H. Wang, S. L. Jacques, and L. Q. Zheng, "MCML-MC modeling of light transport in multi-layered tissues," *Comput. Methods Prog. Biomed.* **47**, 131–146 (1995).
5. J. Thebaut and S. Zavgorodni, "Coordinate transformations for BEAM/EGSnrc Monte Carlo dose calculations of non-coplanar fields received from a DICOM-compliant treatment planning system," *Phys. Med. Biol.* **51**, N441–N449 (2006).
6. J. Zhou and J. Liu, "Numerical study on 3-D light and heat transport in biological tissues embedded with large blood vessels during laser-induced thermotherapy," *Numer. Heat Transfer Part A* **45**, 415–449 (2004).
7. J. W. Tunnell, L. V. Wang, and B. Anvari, "Optimum pulse duration and radiant exposure for vascular laser therapy of dark port wine skin: a theoretical study," *Appl. Opt.* **42**, 1367–1378 (2003).
8. T. J. Pfefer et al., "A three dimensional modular adaptable grid numerical model for light propagation during laser irradiation of skin tissue," *IEEE J. Sel. Topics Quantum Electron.* **2**, 934–942 (1996).
9. D. A. Boas et al., "Three dimensional Monte Carlo code for photon migration through complex heterogeneous media including the adult human head," *Opt. Express* **10**, 159–170 (2002).
10. Q. Fang, "Mesh-based Monte Carlo method using fast ray-tracing in Plücker coordinates," *Biomed. Opt. Express* **1**, 165–175 (2010).
11. T. Binzoni et al., "Light transport in tissue by 3D Monte Carlo: influence of boundary voxelization," *Comput. Methods Prog. Biomed.* **89**, 14–23 (2008).
12. H. Shen and G. Wang, "A tetrahedron-based inhomogeneous Monte Carlo optical simulator," *Phys. Med. Biol.* **55**, 947–962 (2010).
13. H. Jia et al., "Boundary discretization in the numerical simulation of light propagation in skin tissue: problem and strategy," *J. Biomed. Opt.* **20**, 025007 (2015).
14. A. Mohammadi and S. Kinase, "Influence of voxel size on specific absorbed fractions and S-values in a mouse voxel phantom," *Radiat. Prot. Dosim.* **143**, 258–263 (2011).
15. H. Kahn and A. W. Marshall, "Methods of reducing sample size in Monte Carlo computations," *J. Oper. Res. Soc. Am.* **1**, 263–278 (1953).
16. A. Colasanti et al., "Multiple processor version of a Monte Carlo code for photon transport in turbid media," *Comput. Phys. Commun.* **132**, 84–93 (2000).
17. S. V. Patwardhan, A. P. Dhawan, and P. A. Relue, "Monte Carlo simulation of light-tissue interaction: three-dimensional simulation for trans-illumination-based imaging of skin lesions," *IEEE Trans. Biomed. Eng.* **52**, 1227–1236 (2005).
18. N. S. Zolek, A. Liebert, and R. Maniewski, "Optimization of the Monte Carlo code for modeling of photon migration in tissue," *Comput. Methods Prog. Biomed.* **84**, 50–57 (2006).
19. K. Bhan and J. Spanier, "Condensed history Monte Carlo methods for photon transport problems," *J. Comput. Phys.* **225**, 1673–1694 (2007).
20. A. Doronin and I. Meglinski, "Online object oriented Monte Carlo computational tool for the needs of biomedical optics," *Biomed. Opt. Express* **2**(9), 2461–2469 (2011).
21. H. van de Hulst, *Light Scattering by Small Particles*, Dover, New York (1995).
22. S. Prahl, "The adding-doubling method," in *Optical-Thermal Response of Laser Irradiate Tissue*, A. Welch and M. van Gemert, Eds., pp. 101–125, Plenum, New York (1995).
23. R. R. Anderson and J. A. Parrish, "Microvasculature can be selectively damaged using dye lasers: a basic theory and experimental evidence in human skin," *Lasers Surg. Med.* **1**, 263–276 (1981).
24. Y. L. He, Y. B. Tao, and W. Q. Tao, "Numerical study on the performance of wavy fin heat exchangers with different elliptic tube patterns," *Prog. Comput. Fluid Dyn.* **8**, 510–517 (2008).
25. Y. L. He, Y. Y. Tao, and F. Gao, "A new computational model for entire pulse tube refrigerators: model description and numerical validation," *Cryogenics* **49**, 84–93 (2009).
26. D. Miller and A. R. Veitch, "Optical modeling of light distributions in skin tissue following laser irradiation," *Lasers Surg. Med.* **13**, 565–571 (1993).
27. D. J. Smithies and P. H. Butler, "Modeling the distribution of laser-light in port-wine stains with the Monte-Carlo method," *Phys. Med. Biol.* **40**, 701–731 (1995).
28. G. W. Lucassen et al., "Light distributions in a port wine stain model containing multiple cylindrical and curved blood vessels," *Lasers Surg. Med.* **18**, 345–357 (1996).

**Dong Li** earned his PhD degree at Xi'an Jiaotong University, China, in 2013. He is currently a lecturer in the State Key Laboratory of Multiphase Flow in Power Engineering, Xi'an Jiaotong University. He has devoted his efforts to the research of laser light propagation and bio heat transfer model related to laser dermatology.

**Bin Chen** earned his PhD at Xi'an Jiaotong University, China, in 2002. He is currently a full professor and vice director in the State Key Laboratory of Multiphase Flow in Power Engineering, Xi'an Jiaotong University. His research includes photon propagation, heat transfer model, and cryogen spray cooling related to laser dermatology. Now he is serving as an editorial board member of *Journal of Clinical Dermatology and Therapy*.

Biographies for the other authors are not available.